Drastic solid-state luminescent color tuning of an archetypal Ir(III) complex using polyoxometalates and application as vapoluminescence chemosensor

P. Bolle, H. Serier-Brault, R. Génois, E. Faulques, A. Boulmier, O. Oms, M. Lepeltier, J. Marrot, A. Dolbecq, P. Mialane and R. Dessapt

Electronic Supporting Information

Synthetic procedures

All chemicals and reagents were purchased from major chemical suppliers and used as received except $[Ir^{III}(ppy)_2(bpy)](PF_6)$ (hereafter labelled as $[Ir](PF_6)$),[S1] $(TBA)_2[W_6O_{19}]$,[S2] and $(TBA)_4[\alpha\text{-}Mo_8O_{26}]$[S3] ($TBA^+$ = tetrabutylammonium cation) which have been synthesized according to the reported procedures. $((CH_3CH_2)_2NH_2)_2(NH_4)_2[\beta\text{-}Mo_8O_{26}]$ and $(MePPh_3)_2[Mo_4O_{10}(OCH_3)_6]$, which were used as optical references of the $\beta\text{-}[Mo_8O_{26}]^{4-}$ and $[Mo_4O_{10}(OCH_3)_6]^{2-}$ units for solid-state and liquid UV-vis spectroscopy characterizations, were synthesized as previously described in reference S4 and S5, respectively.

Synthesis of $[Ir]_2(TBA)_2[Mo_8O_{26}]$-A ($Ir_2Mo_8$-A). $(TBA)_4[\alpha\text{-}Mo_8O_{26}]$ (0.134 g, 0.062 mmol) and (TBA)Br (0.300 g, 0.930 mmol) were dissolved in acetonitrile (8 mL). The colourless solution (solution 1) was stirred for a few minutes at room temperature. In addition, a second solution (solution 2) is obtained by dissolving $[Ir](PF_6)$ (0.096 g, 0.12 mmol) in acetonitrile (8 mL) at room temperature. Solution 2 was added dropwise to solution 1 under vigorous stirring and the resulting yellow solution was stirred at 30 °C for two hours. The precipitation of a yellow solid happened at the beginning of heating. The mixture was kept at room temperature and then filtered. The powder was washed with few milliters of acetonitrile, then ethanol, and dried in air. The powder was placed in an oven at 100 °C for 24h. The yellow-green solid of **Ir_2Mo_8-A** was cooled at room temperature. Yield in Mo: 81%. *Anal*. Calcd for $C_{96}H_{120}O_{26}N_{10}Mo_8Ir_2$: C, 38.67 ; H, 4.06 ; N, 4.70. Found: C, 38,66 ; H, 4.02 ; N, 4.47. FT-IR (KBr cm^{-1}): 3108 (w), 3084 (m), 3061 (sh), 3033 (m); TBA^+ cation 2961 (s), 2932 (sh), 2872 (s); $[Ir]^+$ complex 1607 (s), 1582 (s), 1560 (w), 1548 (w), 1479 (s), 1437 (sh), 1441 (s), 1420 (s), 1378 (w), 1346 (w), 1311 (m), 1269 (m), 1240 (w), 1230 (m), 1167 (s), 1124 (w), 1105 (w), 1064 (m), 1031 (m); υMo=O, υMo-O-Mo 955 (sh), 943 (vs), 912 (vs), 893 (sh), 843 (s), 808 (w), 797 (sh), 766 (s), 733 (vs), 710 (vs), 665 (s), 629 (sh), 557 (m), 525 (m), 476 (m), 453 (w), 409 (s).

Synthesis of $[Ir]_2(TBA)_2[Mo_8O_{26}]$-B ($Ir_2Mo_8$-B). **$Ir_2Mo_8$-A** (0.034 g, 0.011 mmol) and (TBA)Br (0.050 g, 0.155 mmol) were dissolved in DMF (3 mL). The resulting yellow solution was stirred at 50 °C for one hour, filtered and kept at ambient temperature. Yellow crystals of **Ir_2Mo_8-B** were isolated from the solution after few days. Yield in Mo: 74%. *Anal*. Calcd for $C_{96}H_{120}O_{26}N_{10}Mo_8Ir_2$: C, 38.67 ; H, 4.06 ; N, 4.70. Found: C, 38,37 ; H,

3,93 ; N, 4.40. FT-IR (KBr cm^{-1}): 3101 (m), 3059 (sh), 3032 (m); TBA^+ cation 2961 (s), 2932 (sh), 2872 (s); $[Ir]^+$ complex 1605 (s), 1582 (s), 1560 (w), 1549 (w), 1477 (s), 1439 (sh), 1443 (s), 1418 (s), 1380 (w), 1314 (m), 1269 (m), 1240 (w), 1228 (m), 1163 (s), 1125 (w), 1108 (w), 1065 (m), 1033 (m); υMo=O, υMo-O-Mo 945 (vs), 912 (vs), 893 (sh), 845 (s), 808 (sh), 797 (w), 764 (s), 733 (vs), 712 (vs), 667 (s), 629 (sh), 557 (m), 523 (m), 461 (m), 419 (m).

Synthesis of $[Ir]_4[Mo_8O_{26}]$ (Ir_4Mo_8). $(TBA)_4[\alpha\text{-}Mo_8O_{26}]$ (0.067 g, 0.031 mmol) was dissolved in acetonitrile (4 mL). The colourless solution (solution 1) was stirred for a few minutes at room temperature. In addition, a second solution (solution 2) is obtained by dissolving $[Ir](PF_6)$ (0.099 g, 0.124 mmol) in acetonitrile (4 mL) at room temperature. Solution 2 was added dropwise to solution 1 under vigorous stirring leading to the precipitation of an orange solid. The mixture was stirred at 35 °C for three hours, kept at room temperature, and then filtered. The powder was washed with acetonitrile, ethanol, and dried in air. Then, the powder was placed in an oven at 100 °C for 24h. The orange solid of **Ir_4Mo_8** was cooled at room temperature. Yield in Mo: 75%.

Single-crystals of **Ir_4Mo_8** were obtained according to the following procedure: $(TBA)_4[\alpha\text{-}Mo_8O_{26}]$ (0.033 g, 0.015 mmol) and (TBA)Br (0.075 g, 0.233 mmol) were dissolved in acetonitrile (3 mL). The colourless solution (solution 1) was stirred for a few minutes at room temperature. In addition, a second solution (solution 2) is obtained by dissolving $[Ir](PF_6)$ (0.025 g, 0.031 mmol) in acetonitrile (2 mL) at room temperature. Solution 2 was added dropwise to solution 1 under vigorous stirring. The resulting yellow solution was sealed in a 30 mL Teflon-lined autoclave and was maintained at 110 °C for 40 hours in autogenous pressure conditions. The reactor was then cooled at room temperature and the crystal mixture (orange and yellow crystals) was then filtered and dried in air. Orange crystals of **Ir_4Mo_8** were isolated. *Anal*. Calcd for $C_{128}H_{96}O_{26}N_{16}Mo_8Ir_4$: C, 40.35 ; H, 2.54 ; N, 5.88. Found: C, 39.94 ; H, 2.39 ; N, 5.62. FT-IR (KBr cm^{-1}): 3107 (w), 3078 (w), 3032 (m), 2930 (w) ; $[Ir]^+$ complex 1628 (m), 1607 (s), 1582 (m), 1560 (w), 1549 (w), 1477 (s), 1470 (sh), 1443 (m), 1418 (s), 1369 (sh), 1308 (m), 1267 (m), 1244 (w), 1227 (w), 1161 (m), 1124 (w), 1104 (sh), 1063 (m), 1030 (m), 1020 (sh) ; υMo=O, υMo-O-Mo 951 (m), 922 (vs), 908 (vs), 853 (s), 802 (vs), 775 (w), 760 (s), 743 (m), 733 (m), 662 (vs), 640 (sh), 631 (sh), 557 (m), 505 (w), 417 (m).

Synthesis of $[Ir]_2[Mo_4O_{10}(OCH_3)_6]\cdot 2CH_3OH$ (Ir_2Mo_4). Ir_2Mo_8-A (0.116 g, 0.039 mmol) was dissolved in methanol (15 mL). The resulting yellow solution was stirred at 50 °C for four hours leading to the precipitation of an orange solid. The mixture was kept at room temperature and then filtered. The powder of **Ir_2Mo_4** was washed with methanol, ethanol, and dried in air. Yield in Mo: 92%. Single-crystals of **Ir_2Mo_4** were obtained according to the following procedure: **Ir_2Mo_8-A** (0.035 g, 0.012 mmol) was immersing in methanol (3 mL) and the system was setting to standby at ambient temperature. Orange single-crystals of **Ir_2Mo_4** were isolated from the system after few days. *Anal*. Calcd for $C_{72}H_{74}O_{18}N_8Mo_4Ir_2$: C, 41.03 ; H, 3.54 ; N, 5.32. Found: C, 40.86 ; H, 3.23 ; N, 5.26. FT-IR (KBr cm^{-1}): 3417 (vs), 3103 (w), 3051 (sh), 3032 (w), 2975 (m), 2953 (w), 2894 (m), 2812 (m); $[Ir]^+$ complex 1636 (m), 1603 (s), 1580 (m), 1560 (w), 1545 (w), 1475 (s), 1447 (m), 1437 (sh), 1418 (s), 1313 (m), 1270 (w), 1246 (w), 1225 (w), 1164 (m), 1070 (m), 1040 (s); υMo=O, υMo-O-Mo 1003 (s), 934 (s), 914 (vs), 881 (s), 799 (m), 768 (vs), 755 (sh), 743 (m), 733 (m), 700 (vs), 673 (sh), 652 (sh), 629 (w), 559 (s), 530 (m), 505 (m), 430 (sh), 421 (m).

Synthesis of $[Ir]_2[W_6O_{19}]$ (Ir_2W_6). $(TBA)_2[W_6O_{19}]$ (0.173 g, 0.091 mmol) was dissolved in acetonitrile (7 mL). The colourless solution (solution 1) was stirred for a few minutes at room temperature. In addition, a second solution (solution 2) is obtained by dissolving $[Ir](PF_6)$ (0.150 g, 0.187 mmol) in acetonitrile (4 mL) at room temperature. Solution 2 was added dropwise to solution 1 under vigorous stirring leading to the precipitation of an orange solid. The mixture was stirred at 60 °C for four hours, kept at room temperature, and then filtered. The powder was washed with acetonitrile, ethanol, and dried in air. Then the powder was dissolved in DMF (3 mL). The resulting orange solution was stirred at 50 °C for one hour and then filtered. Single-crystals of Ir_2W_6 were obtained after few days by slow diffusion of ethanol into the solution, at room temperature. Yield in W: 62%.
Anal. Calcd for $C_{64}H_{48}O_{19}N_8W_6Ir_2$: C, 28.25 ; H, 1.78 ; N, 4.12. Found: C, 28.56 ; H, 1.68 ; N, 3.93. FT-IR (KBr cm^{-1}): 3101 (w), 3069 (m), 3040 (w), 2972 (w); $[Ir]^+$ complex 1607 (s), 1582 (s), 1560 (w), 1549 (w), 1477 (s), 1443 (s), 1420 (s), 1313 (m), 1269 (m), 1246 (w), 1229 (w), 1163 (s), 1124 (w), 1105 (w), 1063 (m), 1043 (sh), 1032 (m); υMo=O, υW-O-W 980 (vs), 887 (w), 880 (sh), 820 (vs), 760 (vs), 733 (s), 669 (m), 638 (sh), 631 (w), 586 (s), 559 (sh), 446 (vs), 420 (m).

Physical Measurements. Elemental analyses of the solids were performed by the "Service de microanalyses ICSN CNRS, in Gif sur Yvette (France). FT-IR spectra were recorded in the 4000-400 cm^{-1} range on a BRUKER Vertex equipped with a computer control using the OPUS software. Differential scanning calorimetry (DSC) and thermogravimetric analysis (TGA) were performed by flowing dry argon with a heating and cooling rate of 5°C/min on a SETARAM TG-DSC 111 between 20 and 800°C. Intensity data collections were carried out with a Bruker D8 VENTURE diffractometer equipped with a PHOTON 100 CMOS bidimensional detector using a high brilliance IμS microfocus X-ray Mo Kα monochromatized radiation (λ = 0.71073 Å) for compounds $Ir_2TBA_2Mo_8O_{26}$ (CCDC 1505014) and $Ir_4Mo_8O_{26}$ (CCDC 1505015), and with a Bruker Nonius X8 APEX 2 diffractometer equipped with a CCD bidimensional detector using Mo Kα monochromatized radiation (λ = 0.71073 Å) for compounds Ir_2Mo_4 (CCDC 1505016) and Ir_2W_6 (CCDC 1505017). The absorption corrections were based on multiple and symmetry-equivalent reflections in the data set using the SADABS program[S6] based on the method of Blessing.[S7] The structure were solved by direct methods and refined by full-matrix least-squares using the SHELX-TL package.[S8] The hydrogen atoms were theoretically located on the basis of the conformation of the supporting atoms. Powder X-ray Diffraction spectra were monitored using a D8 Bruker diffractometer in the Bragg-Brentano geometry, equipped with a front germanium monochromator, a copper anode (Cu*K*-L3 radiation λ=1.540598 Å) and a LynxEye PSD detector. NMR spectra were recorded on a Bruker Advance 300 spectrometer operating at 300 MHz for ^1H. Chemical shifts are expressed in parts per million (ppm) downfield from internal TMS. The following abbreviations are used: s, singlet; d, doublet; t, triplet; m, multiplet. Diffuse reflectance spectra were collected at room temperature on a finely ground sample with a Perkin-Elmer Lambda 1050 spectrometer equipped with a 60 mm diameter integrating sphere coated with Spectralon®, a highly reflecting fluoropolymer. Diffuse reflectance was measured from 250 to 1000 nm with a 2 nm step using Halon powder (from Varian) as reference (100% reflectance). The reflectance data were treated by a Kubelka-Munk transformation[S9] to better determine the absorption thresholds. UV-vis absorption spectra in solution were obtained with the same Perkin-Elmer Lambda 1050 spectrometer. Photoluminescence spectra were recorded on a Jobin-Yvon Fluorolog 3 fluorometer equipped with a CCD camera. For photographs, the samples were irradiated with a Fisher Bioblock labosi UV lamp (λ_{exc} = 365 nm, P = 6W). Time-resolved luminescent

experiments were carried out with a regenerative amplified femtosecond Ti:Sapphire laser system (Spectra Physics Hurricane X) producing 100 fs pulses at 800 nm with a repetitive rate of 1 kHz. The laser line is frequency-doubled in a third harmonic generator to give the excitation wavelength λ_{exc} = 400 nm (3.1 eV). The femtosecond laser pulses traces were controlled by an oscilloscope WavePro 950 Lecroy. The emission spectra were temporarily resolved using a high dynamic range Hamamatsu C7700 streak camera of temporal resolution < 20 ps equipped with a readout CCD ORCAII camera Peltier cooled to -60 °C. The excitation density in the samples was adjusted with density filters to avoid sample photodegradation. Powder samples were pressed onto silica glass and studied in the solid state.

Fig. S1. Mixed polyhedral and ball-and-stick representations of the crystal packing in **Ir_2Mo_8-B**. (a) The β-$[Mo_8O_{26}]^{4-}$ units and the TBA^+ cations are associated via electrostatic interactions into $\{(TBA)_2[\beta\text{-}Mo_8O_{26}]^{2-}\}$ layers. (b) The as-defined $\{(TBA)_2[\beta\text{-}Mo_8O_{26}]^{2-}\}$ layers and $[Ir]^+$ complex sheets are stacked along the crystallographic *a* axis. (c) The $[Ir]^+$ complexes form a rectangular paving in the (*bc*) plane. (d) The bpy ligand of the $[Ir]^+$ complex interacts with the POM surfaces via electrostatic interactions with C···O distances shorter than the sum of the van der Waals radii of the concerned atoms, which suggests a high degree of π-π overlapping conducive to efficient intermolecular charge transfer transitions. (blue octahedra = MoO_6; magenta octahedra = IrN_4C_2; grey sphere: carbon; green sphere: nitrogen; orange sphere: oxygen). C···O interactions between $[Ir]^+$ complexes and β-$[Mo_8O_{26}]^{4-}$ units are displayed as dotted lines. The hydrogen atoms are omitted for clarity.

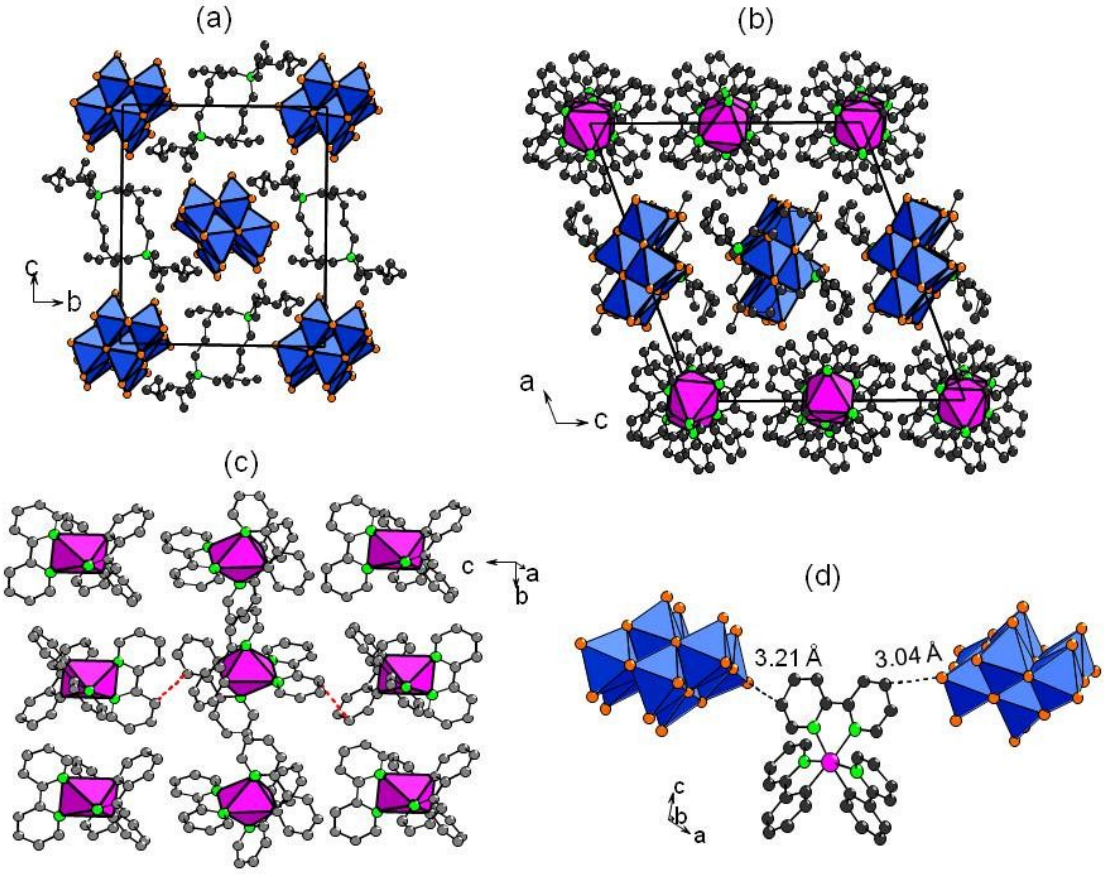

Fig. S2. Mixed polyhedral and ball-and-stick representations of the crystal packing in **Ir_4Mo_8**. (a) α-$[Mo_8O_{26}]^{4-}$ and $[Ir]^+$ complex sheets are stacked along the crystallographic *a* axis. (b) The $[Ir]^+$ complexes form honeycomb-like rubbers ranging along the crystallographic *b* axis, which are separated from each other by α-$[Mo_8O_{26}]^{4-}$ rows also ranging along the crystallographic *b* axis. (c) Four $[Ir]^+$ complexes strongly interact with the α-$[Mo_8O_{26}]^{4-}$ anions via electrostatic interactions with C···O distances shorter than the sum of the van der Waals radii of the concerned atoms, which suggests a high degree of π-π overlapping conducive to efficient intermolecular charge transfer transitions. (blue octahedra = MoO_6; magenta octahedra = IrN_4C_2; grey sphere: carbon; green sphere: nitrogen; orange sphere: oxygen). C···O interactions between $[Ir]^+$ complexes and α-$[Mo_8O_{26}]^{4-}$ units are displayed as dotted lines. The hydrogen atoms are omitted for clarity.

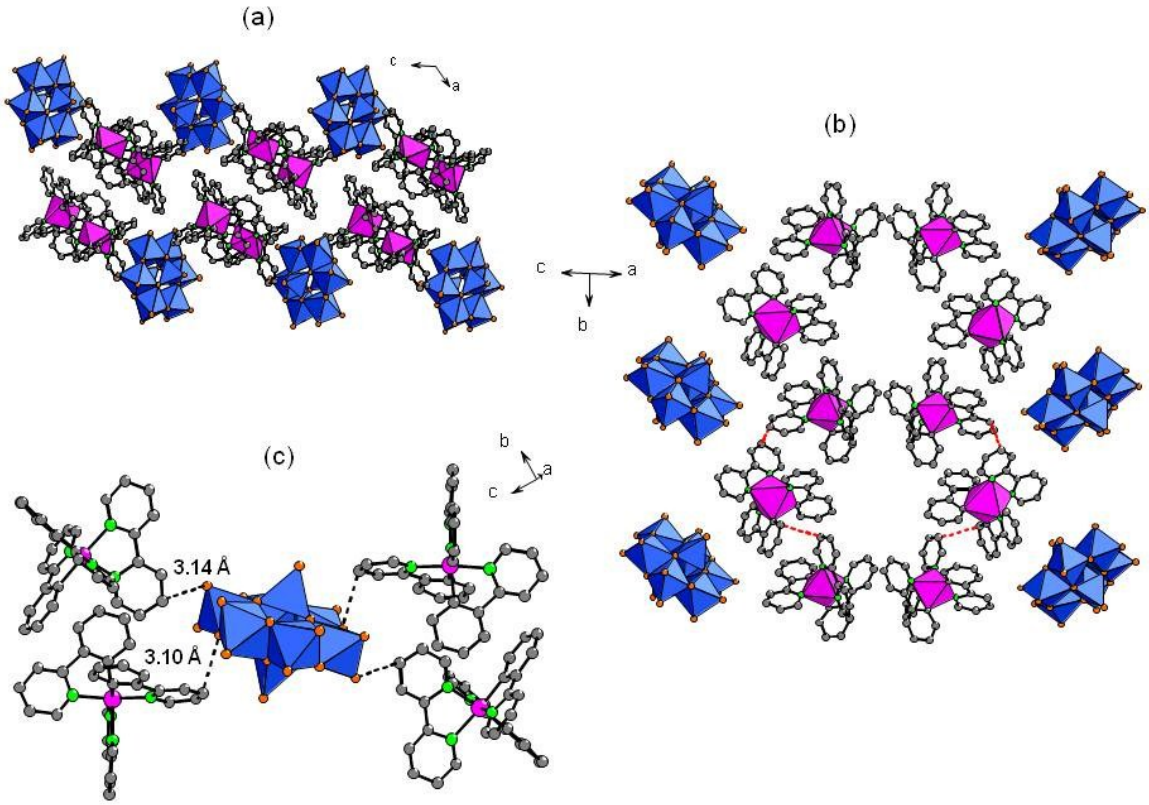

Fig. S3. Mixed polyhedral and ball-and-stick representations of the crystal packing in **Ir_2Mo_4**. (a) $[Mo_4O_{10}(OCH_3)_6]^{2-}$ and $[Ir]^+$ complex sheets are stacked along the crystallographic *a* axis. (b) The $[Ir]^+$ complexes form honeycomb-like layers in the (bc) plane. (c) Two $[Ir]^+$ complexes strongly interact with the POM surfaces via electrostatic interactions with C···O distances shorter than the sum of the van der Waals radii of the concerned atoms, which suggests a high degree of π-π overlapping conducive to efficient intermolecular charge transfer transitions. (blue octahedra = MoO_6; magenta octahedra = IrN_4C_2; grey sphere: carbon; green sphere: nitrogen; orange sphere: oxygen). C···O interactions between $[Ir]^+$ complexes and $[Mo_4O_{10}(OCH_3)_6]^{2-}$ units are displayed as dotted lines. The hydrogen atoms are omitted for clarity.

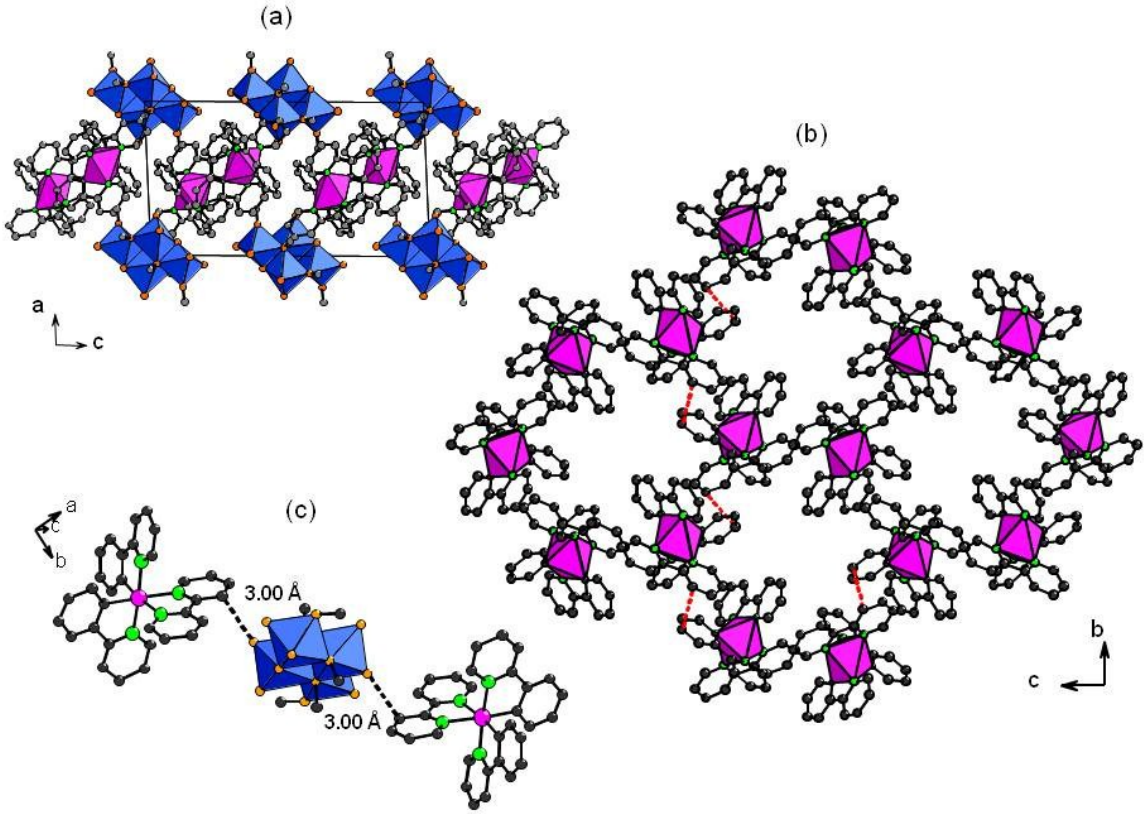

Fig. S4. Mixed polyhedral and ball-and-stick representations of the crystal packing in **Ir_2W_6**. (a) The $[Ir]^+$ complexes form an honeycomb-like channeled architecture. The $[W_6O_{19}]^{2-}$ units form supramolecular chains ranging along the crystallographic *c* axis, and localized inside the hexagonal cavities of the $[Ir]^+$ framework. (c) Six $[Ir]^+$ complexes strongly interact with a $[W_6O_{19}]^{2-}$ unit via electrostatic interactions with C···O distances shorter than the sum of the van der Waals radii of the concerned atoms, which suggests a high degree of π-π overlapping conducive to efficient intermolecular charge transfer transitions. (blue octahedra = MoO_6; magenta octahedra = IrN_4C_2; grey sphere: carbon; green sphere: nitrogen; orange sphere: oxygen). C···O interactions between $[Ir]^+$ complexes and $[W_6O_{19}]^{2-}$ units are displayed as dotted lines. The hydrogen atoms are omitted for clarity.

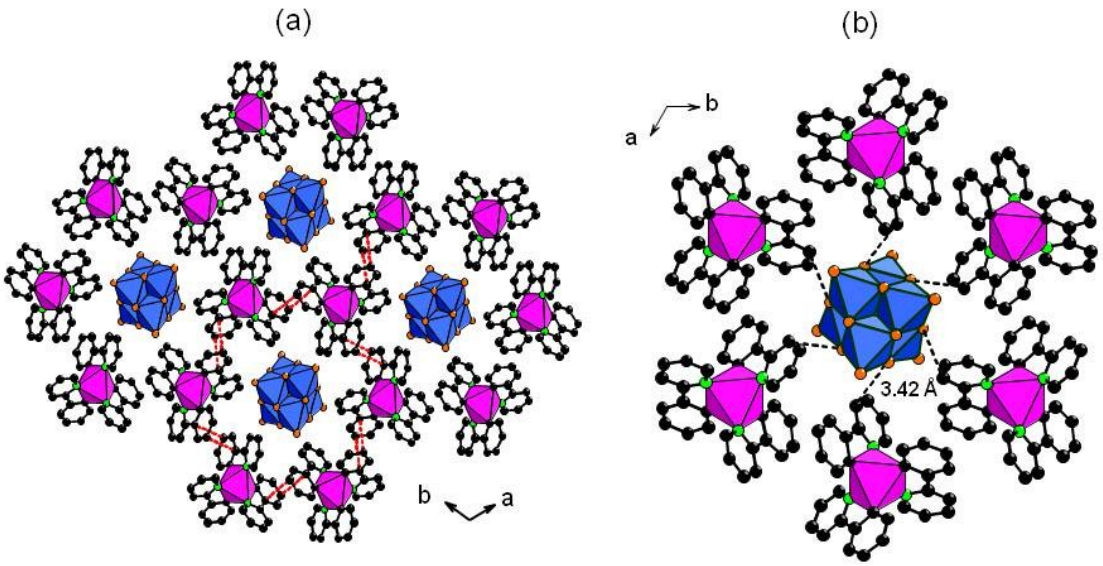

Fig. S5. Comparison of the FT-IR spectra of (a) **Ir_2Mo_8-A**, and (b) **Ir_2Mo_8-B**.

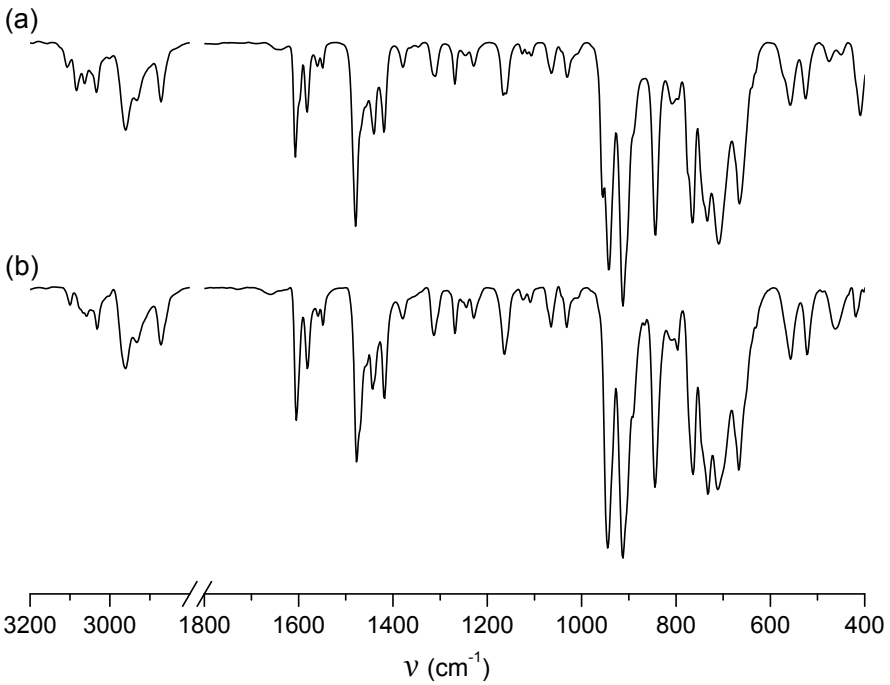

In the spectra of **Ir_2Mo_8-A** and **Ir_2Mo_8-B**, the strong absorption bands in the range 1000-400 cm^{-1} were attributed to the Mo=O and Mo-O-Mo vibration modes of the β-$[Mo_8O_{26}]^{4-}$ anions. Furthermore, the absorption bands in the range 1610-1000 cm^{-1} were mainly assigned to the C-N and C=C aromatic vibration modes of the $[Ir]^+$ complex. Finally, the absorption bands in the range 3000-2850 cm^{-1} were attributed to the C-H alkane vibration mode of the tetrabutylammonium (TBA^+) cations.

Fig. S6. a) ^{1}H NMR spectrum in DMF of **Ir_2Mo_8-A**. The signals denoted by Δ are related to the protons of the TBA cations whereas the signals denoted by ○ correspond to the aromatic protons of the $[Ir]^+$ complex. The integrals of the two sets of signals unambiguously indicate a TBA^+ : $[Ir]^+$ ratio of 1 : 1; b) zoom on the aromatic protons domain; c) zoom on the aliphatic protons domain; d) TGA measurement of **Ir_2Mo_8-A**.

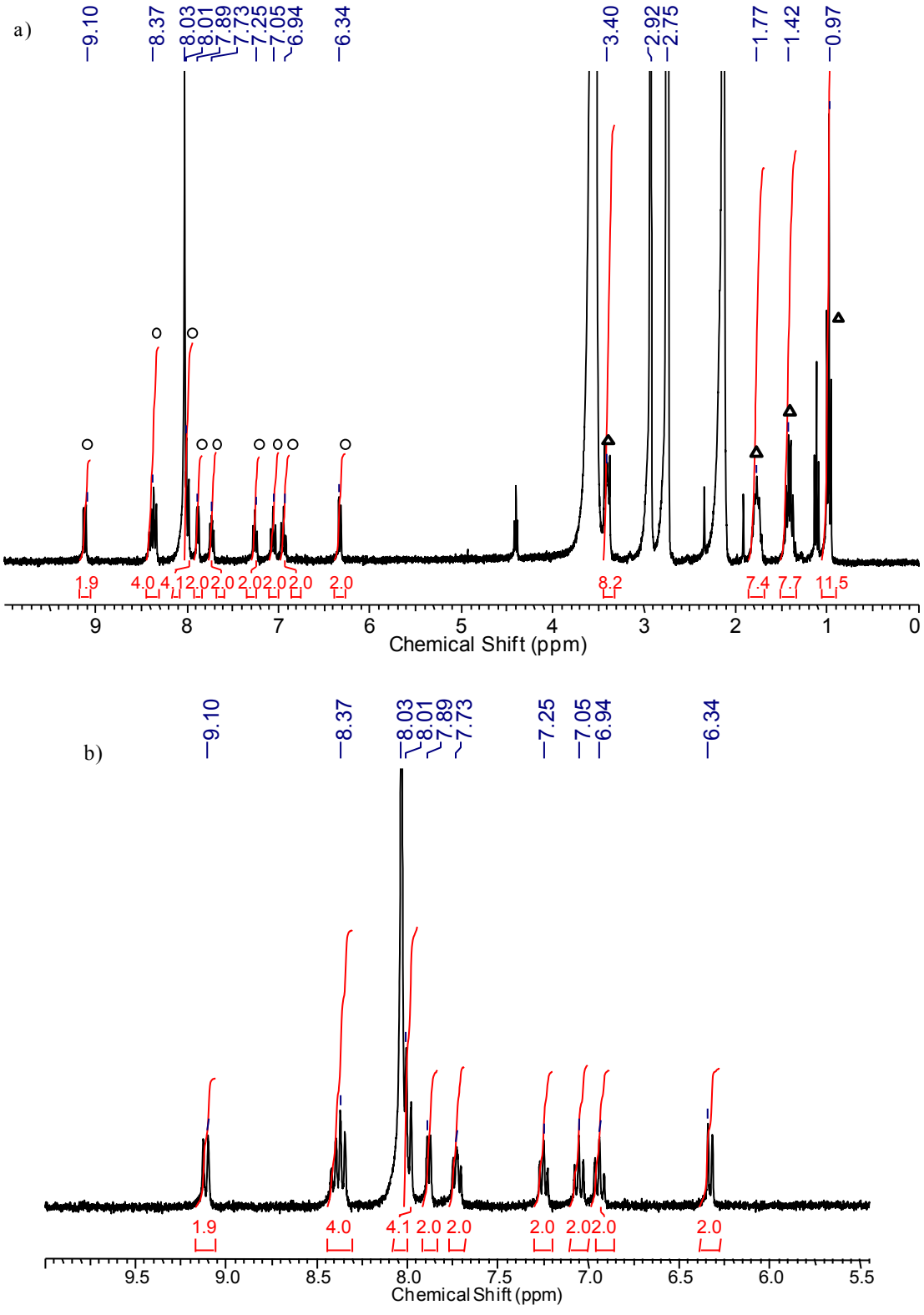

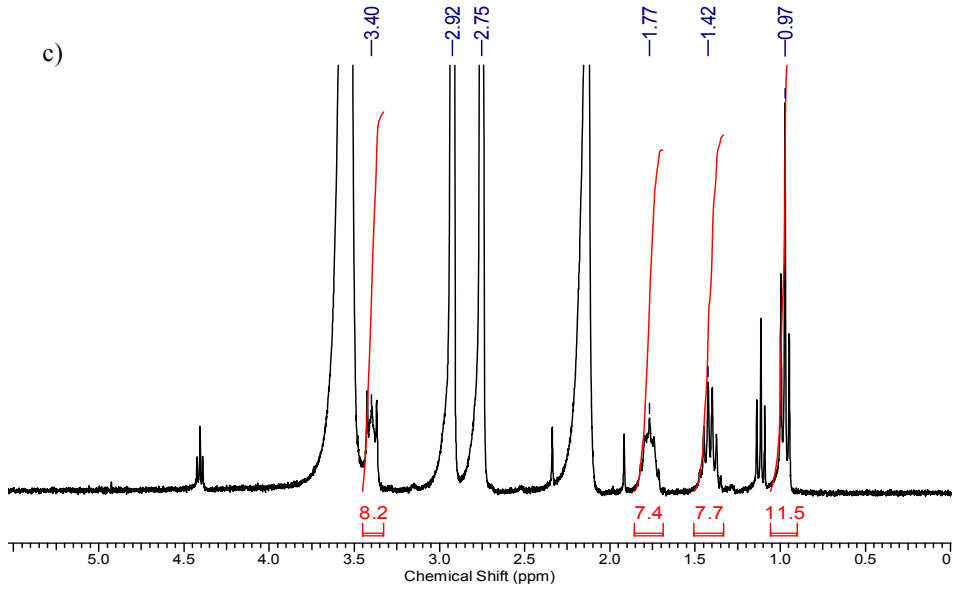

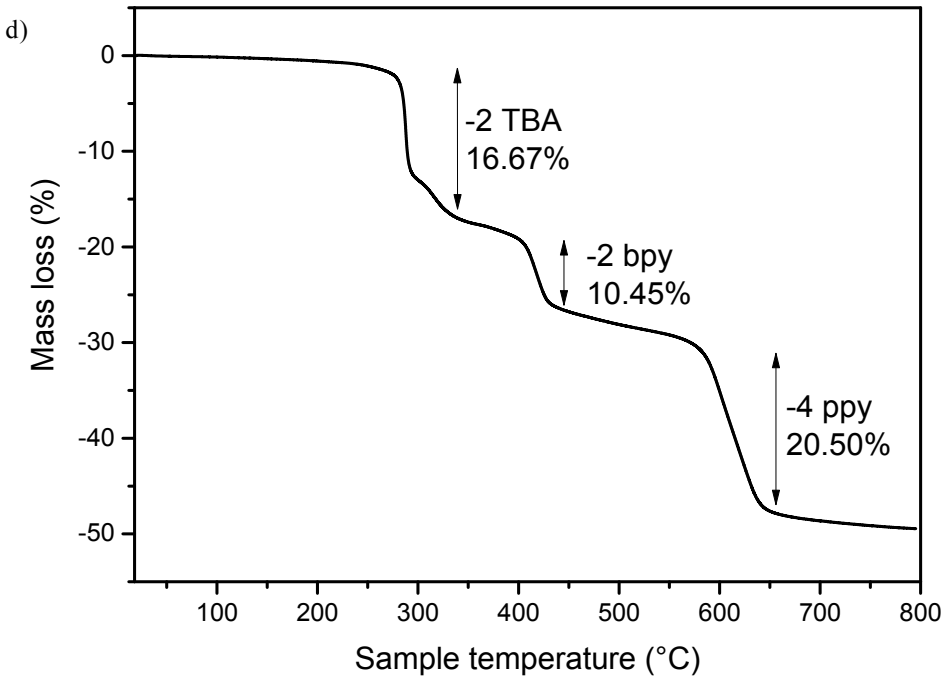

In agreement with the chemical composition, the TGA curve of **Ir_2Mo_8-A** showed three distinct weight losses of 16.67%, 10.45% and 20.50% in the temperature ranges of 250-350, 350-500 and 500-750 °C, respectively, which corresponded to endothermic effects. The first weight loss was attributed to removal of two TBA^+ molecules (theoretical weight loss of 16.2%). The second weight loss was attributed to removal of two bpy molecules (theoretical weight loss of 10.5%). Finally, the third weight loss was attributed to removal of four ppy molecules (theoretical weight loss of 20.7%).

Fig. S7. Comparison of the experimental powder XRD pattern of **Ir_2Mo_8-A** (in red), and of the powder pattern calculated from the structure of **Ir_2Mo_8-B** solved from single-crystal X-ray diffraction data (in black).

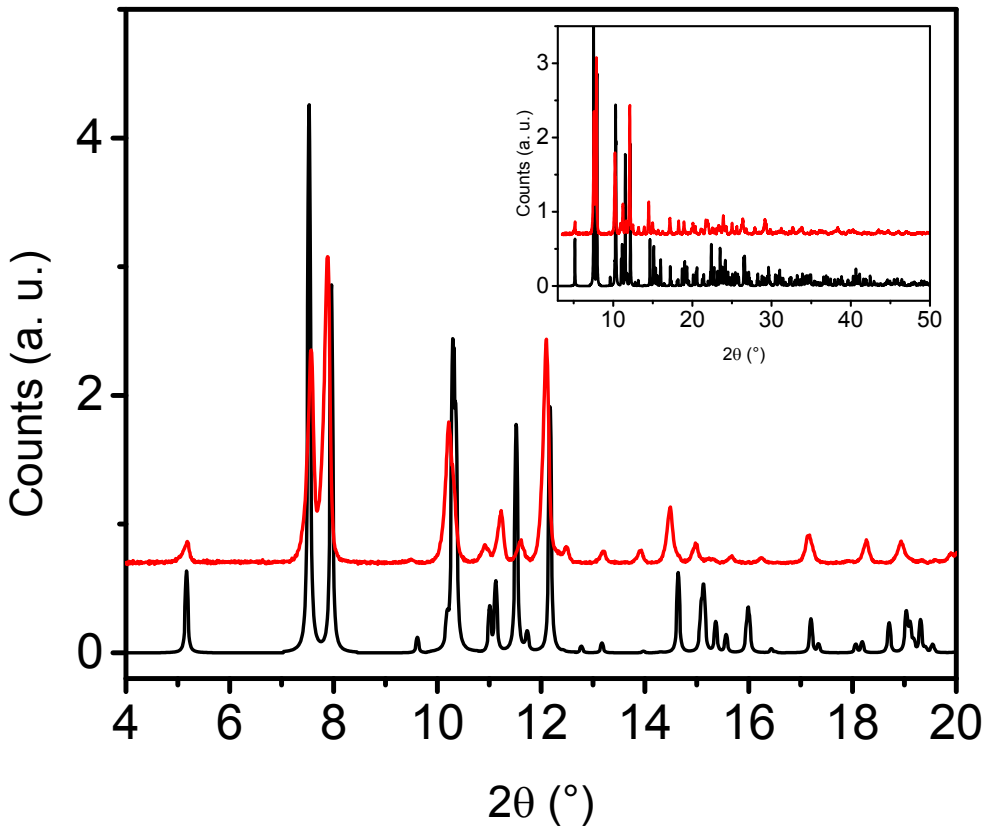

Fig. S8. Kubelka-Munk transformed reflectivity spectra[S9] of (a) **Ir_2Mo_8-A** (black), [Ir](PF_6) (magenta) and $((CH_3CH_2)_2NH_2)_2(NH_4)_2[\beta\text{-}Mo_8O_{26}]$ (blue); (b) **Ir_2Mo_8-B** (black), [Ir](PF_6) (magenta) and $((CH_3CH_2)_2NH_2)_2(NH_4)_2[\beta\text{-}Mo_8O_{26}]$ (blue); (c) **Ir_4Mo_8** (black), [Ir](PF_6) (magenta) and $(TBA)_4[\alpha\text{-}Mo_8O_{26}]$ (blue); (d) **Ir_2Mo_4** (black), [Ir](PF_6) (magenta) and $(MePPh_3)_2[Mo_4O_{10}(OCH_3)_6]$ (blue); (e) **Ir_2W_6** (black), [Ir](PF_6) (magenta) and $(TBA)_2[W_6O_{19}]$ (blue). The absorption denoted by an asterisk in the spectrum of **Ir_2Mo_8-B** was assignable to an intermolecular charge-transfer transition between $[Ir]^+$ and POM molecules, due to their proximity in the crystalline state.

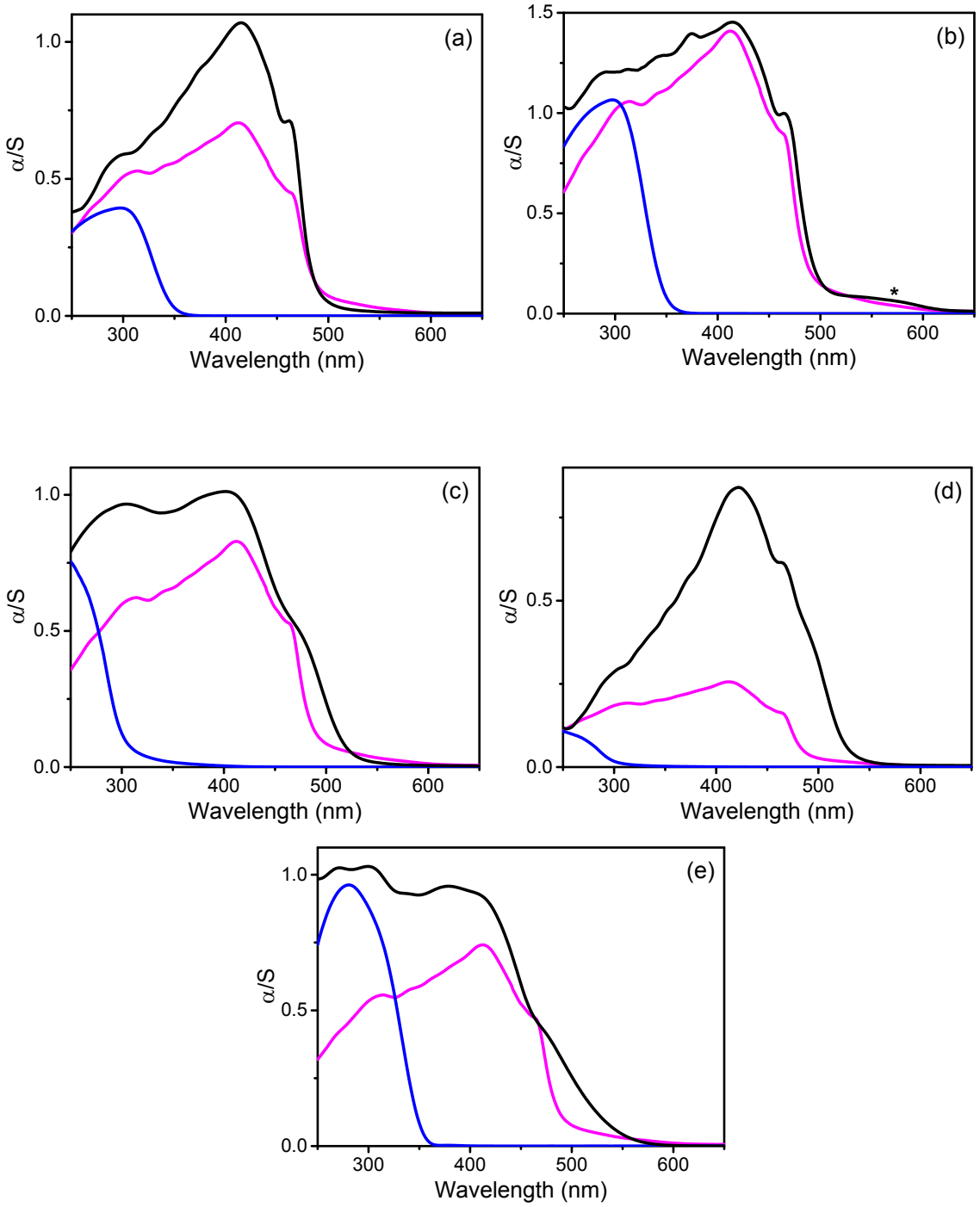

Fig. S9. UV-vis absorption spectra in DMF (2.10^{-5} mol/L) of (a) **Ir_2Mo_8-A** (black), [Ir](PF_6) (red) and $((CH_3CH_2)_2NH_2)_2(NH_4)_2[\beta\text{-}Mo_8O_{26}]$ (blue); (b) **Ir_2Mo_8-B** (black), [Ir](PF_6) (red) and $((CH_3CH_2)_2NH_2)_2(NH_4)_2[\beta\text{-}Mo_8O_{26}]$ (blue); (c) **Ir_4Mo_8** (black), [Ir](PF_6) (red) and $(TBA)_4[\alpha\text{-}Mo_8O_{26}]$ (blue) (d) **Ir_2Mo_4** (black), [Ir](PF_6) (red) and $(MePPh_3)_2[Mo_4O_{10}(OCH_3)_6]$ (blue); (e) **Ir_2W_6** (black), [Ir](PF_6) (red) and $(TBA)_2[W_6O_{19}]$ (blue).

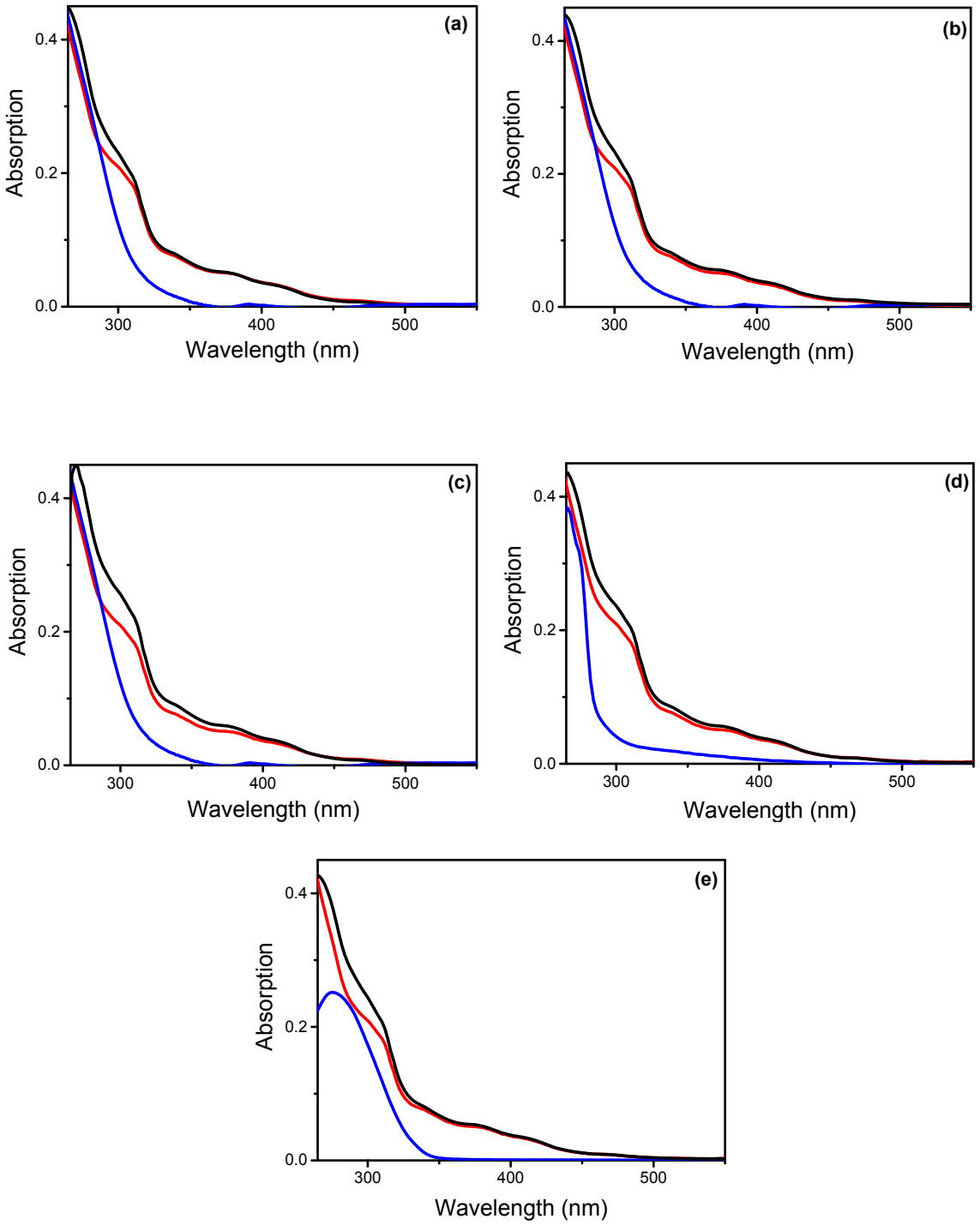

Fig. S10. Temperature-dependence of steady-state PL spectrum of **Ir_2Mo_8-A** monitored at λ_{exc} = 365 nm between 90 K and 300 K.

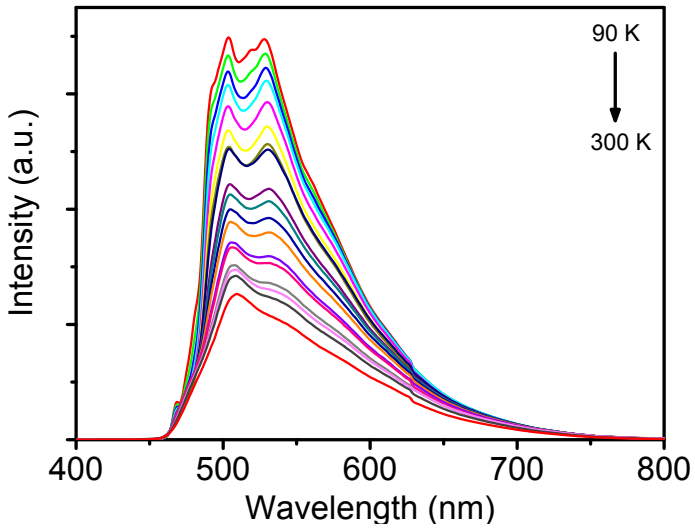

Fig. S11. Temperature-dependence of steady-state PL spectrum of (a) **Ir_4Mo_8**, (b) **Ir_2Mo_4** and (c) **Ir_2W_6** monitored at λ_{exc} = 365 nm between 90 K and 300 K.

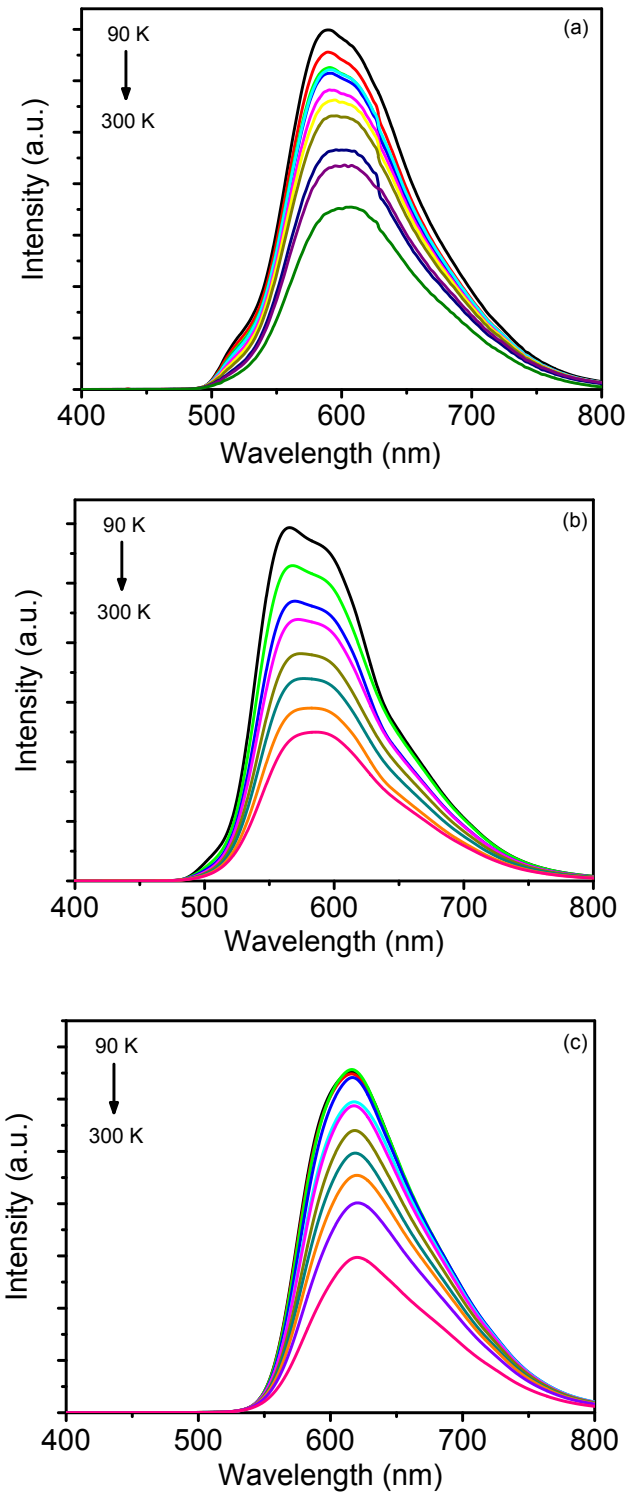

Fig. S12. Time-resolved photoluminescence spectra of **Ir_2Mo_8-B**, **Ir_4Mo_8**, **Ir_2Mo_4**, and [Ir](PF_6) integrated in the sweep ranges 2 ns, 200 ns, and 2 µs. Maximum intensities are normalized to 1.

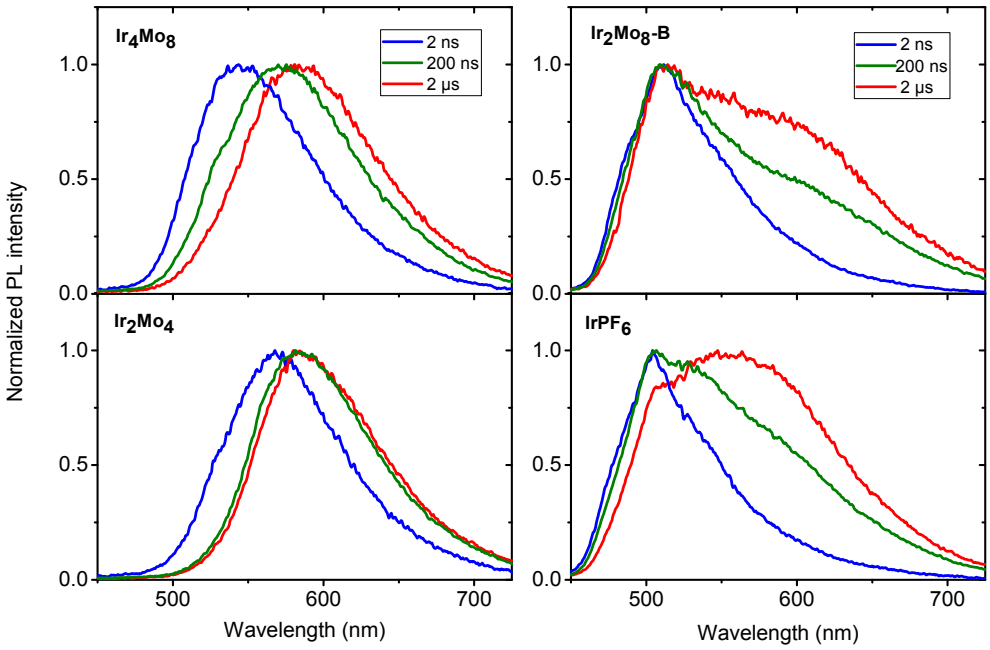

Fig. S13. Photographs of powders of **Ir_2Mo_8-A** (a) before, and (b) after exposure to acetonitrile vapor for 48 h.

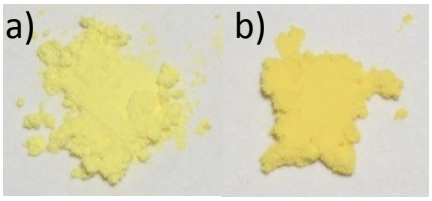

Fig. S14. Evolution of the room temperature steady-state photoluminescence spectrum of **Ir_2Mo_8-A** before (black) and after exposure to acetonitrile vapor for 20 min (red). Colorimetric coordinates of **Ir_2Mo_8-A** (■) before (x=0.324; y=0.554), and (●) after exposure to acetonitrile vapor for 20 min (x=0.332; y=0.551).

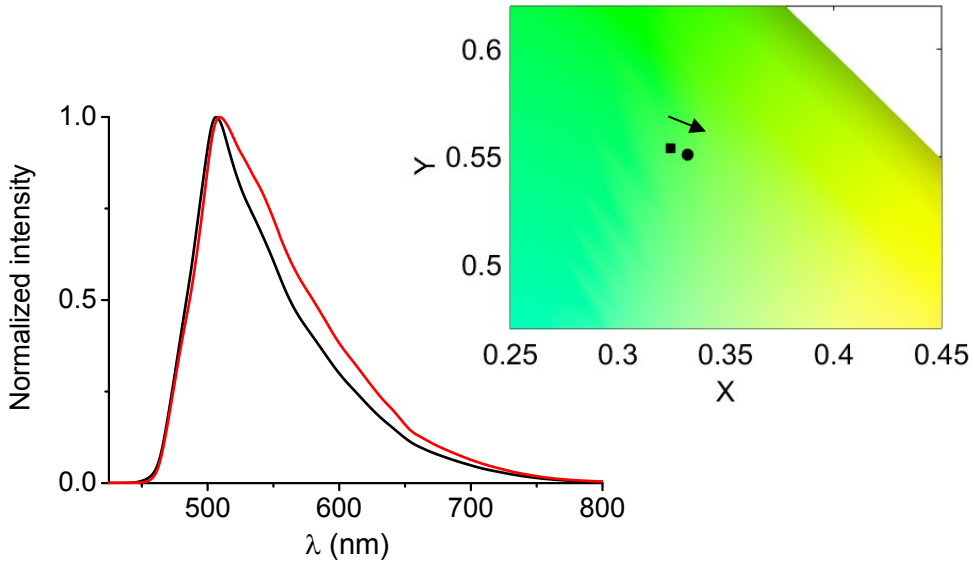

Fig. S15. Normalized Kubelka-Munk transformed reflectivity spectra of **Ir_2Mo_8-A** before (magenta) and after (red) CH_3CN vapor exposure for 24h, **Ir_2Mo_8-B** (black), and **Ir_2Mo_8-A** preliminary exposed to CH_3CN vapor exposure after heating at 120°C for 4h (blue).

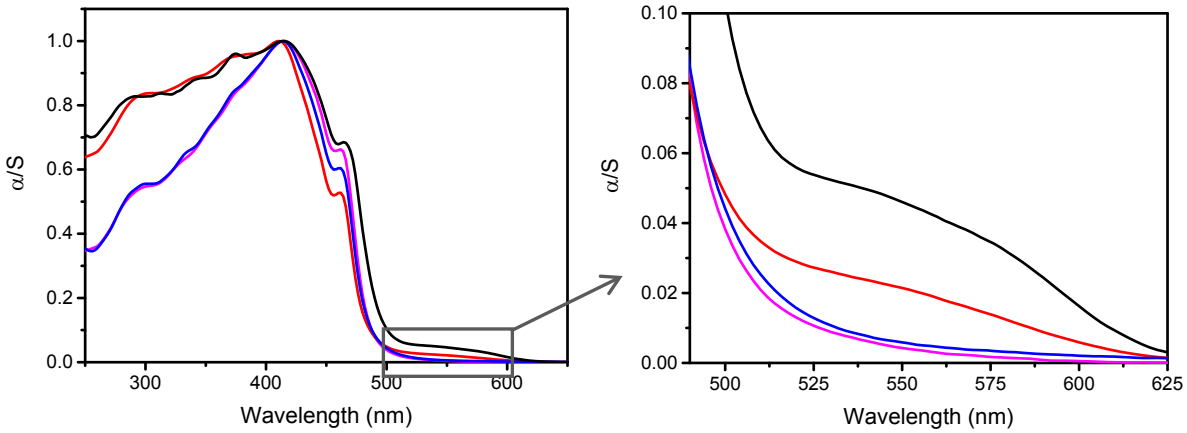

Fig. S16. Comparisons of the experimental powder X-ray diffraction patterns of **Ir_2Mo_8-A** (blue), **Ir_2Mo_8-A** after an exposure for 20 days to vapor of DMF (black), and of the powder pattern calculated from the structure of **Ir_2Mo_8-B** solved from single-crystal X-ray diffraction data (red). The powder XRD pattern of **Ir_2Mo_8-A** after exposure to DMF vapor for 20 days (black) is mainly composed of the XRD pattern of the pristine sample **Ir_2Mo_8-A** together with additional peaks corresponding to the **Ir_2Mo_8-B** sample. The additional peaks are represented by asterisk on the two zoom of the global XRD pattern.

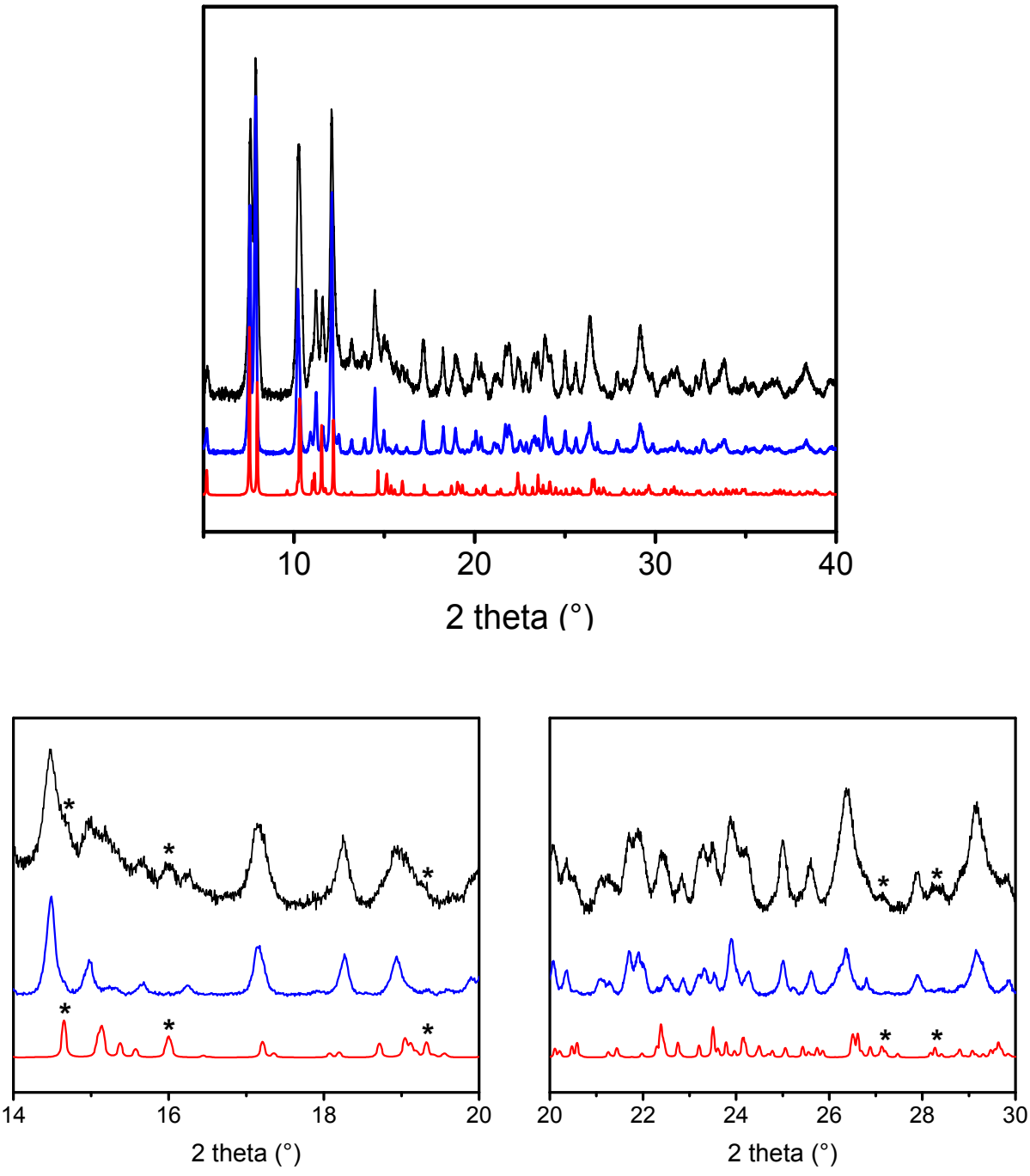

Table S1. X-Ray crystallographic data related to the compounds reported therein.

	Ir_2Mo_8-B	**Ir_4Mo_8**	**Ir_2Mo_4**	**Ir_2W_6**
Empirical formula	$C_{96}H_{120}Ir_2Mo_8N_{10}O_{26}$	$C_{128}H_{96}Ir_4Mo_8N_{16}O_{26}$	$C_{72}H_{66}Ir_2Mo_4N_8O_{18}$	$C_{64}H_{48}Ir_2N_8O_{19}W_6$
Formula weight [g.mol^{-1}]	2981.94	3810.52	2099.48	2716.60
Temperature [K]	200	298	298	298
Crystal system	Monoclinic	Monoclinic	Monoclinic	Trigonal
Space group	$P2_1/c$	$C2/c$	$P2_1/c$	$P\text{-}3c_1$
a [Å]	18.4219(9)	39.372(4)	12.357(1)	15.2896(2)
b [Å]	16.0449(8)	13.8234(12)	13.408(1)	15.2896(2)
c [Å]	18.5278(9)	29.806(3)	21.918(3)	15.6713(4)
β [°]	112.218(2)	125.343(4)	92.173(5)	120
V [Å^3]	5069.8(4)	13232(2)	3628.8(7)	3172.7(1)
Z	2	4	2	2
ρ_{calc} [g cm^{-3}]	1.953	1.913	1.921	2.844
μ [mm^{-1}]	3.646	4.809	4.399	15.087
Data / Parameters	8977/648	11621/820	6475/466	3014/150
R_{int}	0.0546	0.1015	0.0471	0.0680
GOF	1.228	1.116	0.847	1.115
R_1 (>2σ(I))	0.0679	0.0941	0.0227	0.0361
wR_2	0.1457	0.2007	0.0573	0.0982

Table S2. Summary of photophysical properties of the five hybrid POM materials and [Ir](PF_6).

	Absorption			*Steady-state Emission*
Compound	λ_{max} POM[a] (nm)	λ_{max} $[Ir]^+$ (nm)	λ_{CT}[b] (nm)	λ_{max} (nm)[c]
[Ir](PF_6)	-	314, 340, 380, 412, 463	-	585, 505
Ir_2Mo_8_A	296	320, 334, 374, 416, 462	-	505
Ir_2Mo_8_B	296	312, 344, 374, 414, 466	520-625	510, 585
Ir_4Mo_8	250	376, 402, 466	-	594
Ir_2Mo_4	270	320, 350, 372, 422, 464	-	605
Ir_2W_6	275	300, 336, 378, 414, 470	-	621

[a] Lower energy POM LCMT transition. [b] Range of wavelength for the charge-transfer transition. [c] performed at 298 K.

Table S3. Mean decay times τ (ns) of the main peaks obtained from time-resolved photoluminescence (TRPL) spectroscopy for all compounds in the sweep range 2 µs.

TRPL peak(nm) / Compound	510	550	580	600	610
[Ir](PF_6)	101.39	218.11	-	-	-
Ir_2Mo_8-A	78.77	-	237.03	-	-
Ir_2Mo_8-B	75.42	133.9	-	207.24	-
Ir_4Mo_8	-	-	134.27	-	-
Ir_2Mo_4			202.60		
Ir_2W_6	-	-	-	-	120.87

Table S4. Vapochromism and vapoluminescence properties of **Ir_2Mo_8-A** towards solvents.

Solvent	ε[a]	Solubility of Ir_2Mo_8-A	Vapochromism	Vapoluminescence
Heptane	1.92	insoluble	-	-
Ether	4.33	insoluble	-	-
Chloroforme	4.81	insoluble	-	-
THF	7.58	insoluble	-	-
Dichloromethane	8.93	weak	Yes	Yes
Acetone	20.7	weak	Yes	Yes
Methanol	32.7	weak[b]	Yes	Yes
DMF	36.7	high	Yes	Yes
Acetonitrile	37.5	weak	Yes	Yes
Water	80	insoluble	-	-

[a] Dielectric constant. [b] **Ir_2Mo_8-A** was quickly converted into **Ir_2Mo_4**.

References

S1. R. D. Costa, E. Orti, H. J. Bolink, S. Graber, S. Schaffner, M. Neuburger, C. E. Housecroft and E. C. Constable, *Adv. Funct. Mater.*, 2009, **19**, 3456.

S2. C. Sanchez, J. Livage, J.P. Launay and M. Fournier, *J. Am. Chem. Soc.*, 1983, **105**, 6817.

S3. W. G. Klemperer, *Inorg. Synth.*, 1990, **27**, 74.

S4. K. Hakouk, O. Oms, A. Dolbecq, H. El Moll, J. Marrot, M. Evain, F. Molton, C. Duboc, P. Deniard, S. Jobic, P. Mialane and R. Dessapt, *Inorg. Chem*., 2013, **52**, 555.

S5. S. Liu, S. N. Shaikh and J. Zubieta, *Inorg. Chem.*, 1987, **26**, 4303.

S6. G. M. Sheldrick, SADABS, program for scaling and correction of area detector data, University of Göttingen, Germany, 1997.

S7. R. Blessing, *Acta Crystallogr.,* 1995, ***A51***, 33.

S8. G. M. Sheldrick, SHELX-TL version 5.03, Software Package for the Crystal Structure Determination, Siemens Analytical X-ray Instrument Division, Madison, WI USA, 1994.

S9. P. Kubelka and F. Munk, *Z. Tech. Phys*., 1931, **12**, 593.